TE-Wave Penetration Into Finite-Thickness Slotted Circular Cylinder With Lossy and Lossless Inner Coatings

Andriy E. Serebryannikov, *Member, IEEE,* and Alexander I. Nosich, *Fellow, IEEE*

***Abstract*—A technique is developed to study the penetration of a TE-polarized plane wave into perfectly electric conducting cylindrical cavities with multiple apertures, taking into account wall thickness and multilayered inner filling. It is based on an integral representation of the tangential electric field on the slot apertures and the Galerkin method using weighted Gegenbauer polynomials as basis functions. Extensive parametric studies are performed to reveal the main features of the penetrated field in a wide frequency range for single- and double-layer coatings of three types. In particular, the effect of geometric and material parameters on the appearance and attenuation of the cavity resonances is studied. The strongest effect of cylinder thickness on the penetrated field is observed in the vicinity of the peaks of the frequency dependence and must be taken into account, even if the thickness is small.**

***Index Terms*—Cavity-backed aperture, coating, Galerkin method, penetrated field, plane wave.**

I. Introduction

SINCE THE mid-1970's, plane wave scattering by and penetration into the cavity-backed apertures have been extensively studied in connection with various applications, including the development of shielding enclosures, enhancing compatibility of electromagnetic systems, control of radar cross section, and so on. Associated electromagnetic problems have been considered for perfectly electric conducting (PEC) circular (e.g., [1]–[8]), rectangular [9], and arbitrary-shaped [10] and [11] slotted cylindrical shells having zero thickness, by using direct discretizations of integral equations (IEs) [1]–[3], [8]–[11], and semianalytical approaches (e.g., method of analytical regularization) [4]–[7]. Much less attention has been paid to the structures with finite thickness. In particular, scattering of a TM-polarized wave by a thick circular cylinder with a single slot has been studied in [12]. Although the penetrated field has not been considered in [12], the model used therein, which is based on the mode-matching technique, allows doing this. A similar approach has been exploited in [13], where scattering by PEC cylinder with longitudinal corrugations has been studied. Besides, general approaches of scattering by arbitrary-shaped cylinders can be applied to calculate the penetrated field. Among those, it is worth mentioning the approach based on IE for the current distribution on the scatterer surface [14], as well as the approach based on the combination of IE and finite element method [15].

A lot of attention has been paid to the slotted structures with inner or/and outer coatings made of lossless and lossy materials (e.g., [5]–[7]). In [5] and [6], the effect of inner and outer lossy coatings on the far-zone field characteristics has been studied. In [7], penetration of the TM-polarized wave into a circular cylinder with multiple apertures, which is either embedded into or limiting a double-layer coating, has been considered at several fixed frequencies. Penetration of a TE-polarized wave inside a special structure consisting of several concentric slotted circular cylinders of zero thickness was a subject of study in [16].

The main motivation of this study is to control electromagnetic field penetration into multiple cavity-backed apertures. In this paper, we focus on the penetration of the TE-polarized plane wave into a PEC circular cylinder with finite thickness and several apertures. The mathematical treatment is given in Section II. It is based on the modal expansions of the scattered and penetrated fields and on an integral representation of the tangential electric field on the slot apertures. Discretization is performed using the Galerkin method with weighted Gegenbauer polynomials as basis functions. The developed model sets no limitation on the slot width and takes into account a multilayered inner filling.

Thanks to the circular boundaries of the PEC shell and inner layers, our approach avoids discretization of a volume domain that is required in the method from [15]. Instead, it leads to integral-type relations on the surface of the slot apertures discretized with a proper account of the edge behavior. This is similar to [7], where IEs were obtained for the currents on the infinitely thin strips (circular segments), and field behavior at the edges was taken into account. Note that in the previous studies of finite-thickness circular geometries [12]–[14], the edge effect was neglected. Besides, our model is free of restriction of [13], where the slots were located periodically. In Section III, we present numerical simulations performed for finite-thickness cylinders with single- and double-layer coatings of three types. The emphasis is on the effect of shell thickness on the penetrated field and on that how the penetrated field can be enhanced due to the cavity resonances and how to compensate this enhancement. Time dependence $e^{i\omega t}$ is assumed and suppressed throughout this paper.

Manuscript received May 25, 2004; revised August 30, 2005.

A. E. Serebryannikov is with the Arbeitsbereich Hochfrequenztechnik, Technische Universitaet Hamburg–Harburg, D-21071 Hamburg, Germany, on leave from the Institute of Radio Astronomy, National Academy of Sciences of Ukraine, 61002 Kharkov, Ukraine (e-mail: aesnew@hotmail.com).

A. I. Nosich is with the Institute of Radio-Physics and Electronics, National Academy of Sciences of Ukraine, 61085 Kharkov, Ukraine (e-mail: alex@emt.kharkov.ua).

Digital Object Identifier 10.1109/TEMC.2005.859058

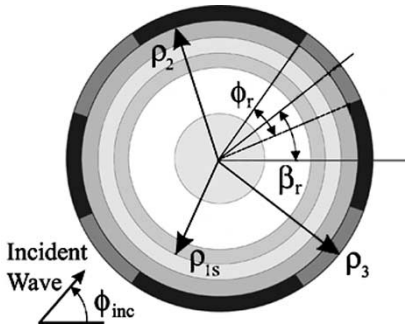

Fig. 1. Slotted circular metallic cylinder with finite thickness and inside coating.

II. Theory

Fig. 1 shows the cross section of a PEC finite-thickness circular cylinder with N sectorial slots. The angular width and angular coordinate of the r th slot center are denoted by ϕ_r and β_r, respectively, $r = 0, 1, \ldots, N-1$. The inner and outer radii of metallic shell are denoted by ρ_2 and ρ_3. A multilayered filling may contain both lossy and lossless layers. In general, it consists of M layers ($\rho_{1s} \le \rho \le \rho_{1,s+1}, s = 1, 2, \ldots, M, \rho_{1,M+1} = \rho_2$) with the relative permittivity ε_{1s} and permeability μ_{1s}. Some of these layers are allowed to show $\varepsilon = \varepsilon_0 = 1$ and $\mu = \mu_0 = 1$ which correspond to the free space. The most inner (circular) subdomain ($s = 0, \rho \le \rho_{11}$) may be metallic or dielectric. Each slot domain ($\rho_2 \le \rho \le \rho_3, \beta_r - \phi_r/2 \le \phi \le \beta_r + \phi_r/2$) is filled with a lossy or lossless material having parameters ε_{2r} and μ_{2r}. The incidence angle $\phi_{\rm inc} = 0$ is assumed throughout the paper, except for the case when the reciprocity theorem is verified.

To satisfy the Helmholtz equation, the H_z component inside the cylinder inner layers (domain I) is expressed in terms of the series

$$H_z^{\rm Is} = \sum_{m=0}^{\infty} \left(A_{ms}^c \cos m\phi + A_{ms}^s \sin m\phi\right) J_m(k_{1s}\rho) + \left(B_{ms}^c \cos m\phi + B_{ms}^s \sin m\phi\right) Y_m(k_{1s}\rho). \quad (1)$$

Here, $s = 0, 1, \ldots M, \rho_{1s} \le \rho \le \rho_{1,s+1}, \rho_{1,M+1} = \rho_2, \rho_{10} = 0, k_{1s} = k_0\sqrt{\varepsilon_{1s}\mu_{1s}}$ is the wavenumber of the sth layer, k_0 is the free-space wavenumber, J_m and Y_m are the mth-order Bessel and Neumann functions, and the upper indices c and s indicate the relation of unknown coefficients to the cosine and sine dependence in ϕ, respectively. In the case of the central subdomain ($s = 0$), $B_{m0}^c = B_{m0}^s \equiv 0$. If it is filled with metal, $B_{m1}^{c,s} = -A_{m1}^{c,s} J_m'(k_{11}\rho_{11})/Y_m'(k_{11}\rho_{11})$, where the prime denotes the derivative with respect to the argument.

In each slot (domain II)

$$H_z^{{\rm II}(r)} = \sum_{n=0}^{\infty} \left[D_{nr} J_{\nu_{nr}}(\kappa_{2r}\rho) + E_{nr} Y_{\nu_{nr}}(\kappa_{2r}\rho)\right] \times \cos[\nu_{nr}(\phi - \beta_r + \phi_r/2)] \quad (2)$$

where $\kappa_{2r} = k_0\sqrt{\varepsilon_{2r}\mu_{2r}}$ and $\nu_{nr} = \pi n/\phi_r$. Finally, in the outer space (domain III) the scattered field series has to match the condition of radiation, hence

$$H_z^{\rm III} = \exp(-ik_0\rho\cos\phi) + \sum_{m=0}^{\infty} \left(V_m^c \cos m\phi + V_m^s \sin m\phi\right) H_m^{(2)}(k_0\rho) \quad (3)$$

where $H_m^{(2)}$ is the mth-order second-kind Hankel function and $i = \sqrt{-1}$.

To connect the unknown coefficients $A_{mM}^{c,s}, B_{mM}^{c,s}, D_{nr}, E_{nr}$, and $V_m^{c,s}$ with the incident wave, we use the boundary conditions for H_z and E_ϕ at $\rho = \rho_2, \rho_3$. The coefficients $A_{ms}^{c,s}$ at $s < M$ and $B_{ms}^{c,s}$ at $s \le M$ are excluded from consideration by using the boundary conditions at $\rho = \rho_{1s}$ and the orthogonality of the trigonometric functions. According to the Galerkin method, the angular dependence of E_ϕ on both apertures of each slot ($\rho = \rho_2, \rho_3, \beta_r - \phi_r/2 \le \phi \le \beta_r + \phi_r/2, r = 0, 1, \ldots, N-1$) is presented as follows:

$$E_\phi^{\rm I}(\rho_2, \phi) = E_\phi^{{\rm II}(r)}(\rho_2, \phi) = iW_0 \sum_{j=1}^{\infty} a_{jr}\Theta_j(x_r) \quad (4)$$

$$E_\phi^{\rm III}(\rho_3, \phi) = E_\phi^{{\rm II}(r)}(\rho_3, \phi) = iW_0 \sum_{j=1}^{\infty} b_{jr}\Theta_j(x_r). \quad (5)$$

Here, W_0 is the free-space impedance, a_{jr} and b_{jr} are unknown coefficients, Θ_j are the basis functions, and $x_r = \phi - \beta_r$.

Using the orthogonality of the sine and cosine functions and the relation between E_ϕ and H_z, we express the coefficients $A_{mM}^{c,s}, B_{mM}^{c,s}, D_{nr}, E_{nr}$, and $V_m^{c,s}$ through $\tilde{X}_{Lr}^{{\rm I}c,s} = \sum_{j=1}^{\infty} c_{jr}\Omega_{jr}^{{\rm I}c,s}$ and $\tilde{X}_{Lr}^{\rm II} = \sum_{j=1}^{\infty} c_{jr}\Omega_{jr}^{\rm II}$. Here, $L = 2$ and $L = 3$ correspond to $\rho = \rho_2$ and $\rho = \rho_3$, respectively, c_{jr} means either a_{jr} ($L = 2$) or b_{jr} ($L = 3$), $\Omega_{jr}^{{\rm I}c,s} = \int_{\alpha_r} \Theta_j(x_r)\Psi_m^{c,s}(x_r + \beta_r)dx_r$, $\Omega_{jr}^{\rm II} = \int_{\alpha_r} \Theta_j(x_r)\cos[\nu_{nr}(x_r + \phi_r/2)]\,dx_r$, where α_r is the aperture of the r th slot, so that $-\phi_r/2 \le x_r \le \phi_r/2$, $\Psi_m^c(y) = \cos(my)$, and $\Psi_m^s(y) = \sin(my)$.

Substituting the obtained coefficients into (1)–(3), using the field continuity at the slot apertures, that is, conditions $H_z^{\rm I}(\rho_2, \phi) = H_z^{{\rm II}(r)}(\rho_2, \phi)$ and $H_z^{\rm III}(\rho_3, \phi) = H_z^{{\rm II}(r)}(\rho_3, \phi)$, and applying the Galerkin method, we arrive at the following set of linear algebraic equations:

$$\sum_{j=1}^{\infty}\sum_{s=0}^{N-1}\left\{\delta_r^s \sum_{n=0}^{\infty}\Lambda_{nr}\left(a_{jr}\vartheta_{nr}^{(+)} - b_{jr}\tau_{nr}^{(+)}\right) - a_{js}h_{jslr}(T) - b_{js}h_{jslr}(R)\right\} = e_{lr} \quad (6)$$

$$\sum_{j=1}^{\infty}\sum_{s=0}^{N-1}\left\{\delta_r^s \sum_{n=0}^{\infty}\Lambda_{nr}\left(a_{jr}\vartheta_{nr}^{(-)} - b_{jr}\tau_{nr}^{(-)}\right) + a_{js}h_{jslr}(T) - b_{js}h_{jslr}(R)\right\} = e_{lr} \quad (7)$$

where δ_r^s is the Kronecker delta, $r = 0, 1, \ldots, N-1$, $l = 1, 2, \ldots, \vartheta_{nr}^{(\pm)} = \theta P_{nr} \pm U_{nr}, \theta = \rho_2/\rho_3$, and $\tau_{nr}^{(\pm)} =$

$Q_{nr} \pm P_{nr}$ [see (25)–(27)]. The factors Λ_{nr}, h_{jslr}, and e_{lr} are given by

$$\Lambda_{nr} = \left(2-\delta_n^0\right) W_0 F_{jrlr} \big/ \left(\phi_r W_{2r}\right) \tag{8}$$

$$h_{jslr}(X) = \sum_{m=0}^{\infty} \varsigma_m X_m \left[\left(\Omega_{js}^{\mathrm{I}c}\Omega_{lr}^{\mathrm{I}c} + \Omega_{js}^{\mathrm{I}s}\Omega_{lr}^{\mathrm{I}s}\right)\cos(m\gamma_{rs}) + \left(\Omega_{js}^{\mathrm{I}c}\Omega_{lr}^{\mathrm{I}s} - \Omega_{js}^{\mathrm{I}s}\Omega_{lr}^{\mathrm{I}c}\right)\sin(m\gamma_{rs})\right] \tag{9}$$

$$e_{lr} = \sum_{m=0}^{\infty} \left(2-\delta_m^0\right)(-i)^m S_m \times \left[\Omega_{lr}^{\mathrm{I}c}\cos(m\beta_r) - \Omega_{lr}^{\mathrm{I}s}\sin(m\beta_r)\right]. \tag{10}$$

Here, $\gamma_{rs} = \beta_s - \beta_r, \varsigma_m = (2-\delta_m^0)/(2\pi)$ if $X = R$ and $\varsigma_m = (2-\delta_m^0)W_0/(2\pi W_{1M})$ if $X = T$, where W_{1M} means impedance of Mth layer. $F_{jrlr} = \Omega_{lr}^{\mathrm{II}}\Omega_{jr}^{\mathrm{II}}$ in (8) and $\Omega_{js}^{\mathrm{I}c,s}$ in (9) and (10) depend on the type of basis functions used in (4) and (5). To adequately take into account the field behavior at the edges, we use the weighted Gegenbauer polynomials as the basis functions

$$\Theta_{jr}(x_r) = (\phi_r/2)^{2\eta}\Lambda_r G_{j-1}^{1/2+\eta}(2x_r/\phi_r) \tag{11}$$

where $G_{j-1}^{1/2+\eta}$ are the Gegenbauer polynomials of the $(j-1)$th order and $\Lambda_r = [1-(2x_r/\phi_r)^2]^{\eta}$ is the weight factor [17]. The sets of even and odd Gegenbauer polynomials are orthogonal with the weight factor, which takes into account the Meixner condition at a rectangular edge in explicit form if setting $\eta = -1/3$ [18]. The interval of the orthogonality is matched with a slot aperture. The corresponding closed-form expressions for F_{jrlr} and $\Omega_{js}^{\mathrm{I}c,s}$ can be obtained using table integrals. They are given, within normalization constant, by (11)–(15) from [19].

Information about the radial geometry of domains I and III is contained in the coefficients

$$R_m = H_m^{(2)}(k_0\rho_3) \Big/ H_m^{(2)'}(k_0\rho_3) \tag{12}$$

$$S_m = J_m(k_0\rho_3) - J_m'(k_0\rho_3)R_m \tag{13}$$

$$T_m = I_m(k_{1M}\rho_2)/I_m'(k_{1M}\rho_2). \tag{14}$$

Here

$$I_m(y) = J_m(y) - K_m Y_m(y) \tag{15}$$

where the coefficient $K_m = -B_{mM}^{c,s}/A_{mM}^{c,s}$ takes into account the multilayered interior of the cylinder at $\rho \le \rho_2$. To calculate K_m in the case of $M > 1$, we apply the recurrent formulas

$$\hat{B}_{m,s+1} = u_s\hat{A}_{ms} + w_s\hat{B}_{ms} - \hat{A}_{m,s+1} \tag{16}$$

$$f_s\hat{A}_{ms} + g_s\hat{B}_{ms} = y_{s+1}\hat{A}_{m,s+1} \tag{17}$$

where $\hat{A}_{ms} = A_{ms}J_m(k_{1s}\rho_{1s})$ and $\hat{B}_{ms} = B_{ms}Y_m(k_{1s}\rho_{1s})$, the upper index c or s is omitted, and the coefficients u_s, w_s, y_{s+1}, and f_s are given by

$$u_s = J_m(z_{s,s+1})/J_m(z_{ss}) \tag{18}$$

$$w_s = Y_m(z_{s,s+1})/Y_m(z_{ss}) \tag{19}$$

$$y_{s+1} = -2/[\pi z_{s+1,s+1}J_m(z_{s+1,s+1})Y_m(z_{s+1,s+1})] \tag{20}$$

$$f_s = \tilde{u}_s W_s/W_{s+1} - u_s Y_m'(x_{s+1,s+1})/Y_m(x_{s+1,s+1}) \tag{21}$$

with $z_{s,s+1} = k_{1s}\rho_{1,s+1}$ and $\tilde{u}_s = J_m'(z_{s,s+1})/J_m(z_{ss})$. Coefficients g_s are obtained from (21) by replacing f_s with g_s, u_s with w_s and $\tilde{u}_s$ with $\tilde{w}_s = Y_m'(z_{s,s+1})/Y_m(z_{ss})$. Because $\hat{B}_{m1}/\hat{A}_{m1}$ is known from the boundary conditions at $\rho = \rho_{11}$, $\hat{A}_{m2}/\hat{A}_{m1}$ is first calculated from (17). Then, $\hat{B}_{m2}/\hat{A}_{m1}$ is calculated from (16), and finally, $\hat{B}_{m2}/\hat{A}_{m2}$ is obtained. This procedure is repeated until s reaches $s = M$. As a result, we obtain

$$K_m = -\hat{B}_{mM}J_m(k_{1M}\rho_{1M})/[\hat{A}_{mM}Y_m(k_{1M}\rho_{1M})]. \tag{22}$$

Once the coefficients a_{jr} and b_{jr} are found from (6) and (7), the field in any domain can be calculated. The coefficients needed to calculate the penetrated field are given as

$$A_{mM}^{c,s} = \varsigma_m \sum_{j=1}^{\infty}\sum_{r=1}^{N-1} a_{jr}\left[\Omega_{jr}^{c}\Psi_m^{c,s}(\beta_r) - p^{c,s}\Omega_{jr}^{s}\Psi_m^{s,c}(\beta_r)\right] \big/ I_m'(k_{1M}\rho_2) \tag{23}$$

and

$$B_{mM}^{c,s} = -K_m A_{mM}^{c,s}. \tag{24}$$

In (23), ς_m is the same as in (9) at $X = T, p^c = 1$, and $p^s = -1$. To calculate the coefficients $A_{mM}^{c,s}$ and $B_{mM}^{c,s}$ at $s < M$, one should again use (16)–(21) modified in such a manner that $\hat{B}_{ms}$ is excluded from either (16) or (17).

The radial geometry of the slots is taken into account in (6) and (7) by the factors

$$U_{nr} = Z_{\nu_{nr}}(\kappa_{2r}\rho_2, \kappa_{2r}\rho_3)/\tilde{Z}_{\nu_{nr}}(\kappa_{2r}\rho_2, \kappa_{2r}\rho_3) \tag{25}$$

$$P_{nr} = 2/[\pi\kappa_{2r}\rho_2\tilde{Z}_{\nu_{nr}}(\kappa_{2r}\rho_2, \kappa_{2r}\rho_3)] \tag{26}$$

$$Q_{nr} = Z_{\nu_{nr}}(\kappa_{2r}\rho_3, \kappa_{2r}\rho_2)/\tilde{Z}_{\nu_{nr}}(\kappa_{2r}\rho_2, \kappa_{2r}\rho_3) \tag{27}$$

where $Z_\tau(z_1, z_2) = J_\tau(z_1)Y_\tau'(z_2) - Y_\tau(z_1)J_\tau'(z_2)$ and $\tilde{Z}_\tau(z_1, z_2) = \frac{d}{dz}[Z_\tau(z, z_2)]|_{z=z_1}$. Calculation of these coefficients can be simplified if cylinder is thin and/or slots are narrow as compared with the wavelength. Assume $\nu_{1r} = \pi/\phi_r \gg 1$ and $1-(\rho_2/\rho_3)^{\nu_{1r}} \ll 1$. Then, using the large-order asymptotics of cylindrical functions [20] and applying the Taylor series expansion to the obtained formulas, we obtain $(n > 0)$

$$Q_{nr} + P_{nr} \approx -2x_{3r}^2 \big/ \left(\delta_r\nu_{nr}^2\right) \tag{28}$$

$$\theta P_{nr} + U_{nr} \approx -2x_{2r}x_{3r} \big/ \left(\delta_r\nu_{nr}^2\right) \tag{29}$$

$$Q_{nr} - P_{nr} \approx -\delta_r/2 \tag{30}$$

$$\theta P_{nr} - U_{nr} \approx \delta_r x_{2r}/(2x_{3r}) \tag{31}$$

where $x_{2r} = \kappa_{2r}\rho_2, x_{3r} = \kappa_{2r}\rho_3$, and $\delta_r = x_{3r} - x_{2r}$. We refer to these expressions as the narrow-slot–thin-wall (NSTW) approximation.

III. Numerical Results and Discussion

The extensive numerical simulations have been performed using the equations obtained in Section II, for the dielectric fillings of three types: single-layer lossy coating made of poly-2.5-dichlorostyrene $(\varepsilon_{11} = 7.3, \mu_{11} = 0.91 - 0.32i)$ [21], single-layer lossy coating made of shellac, natural XL ($\varepsilon_{11} =$

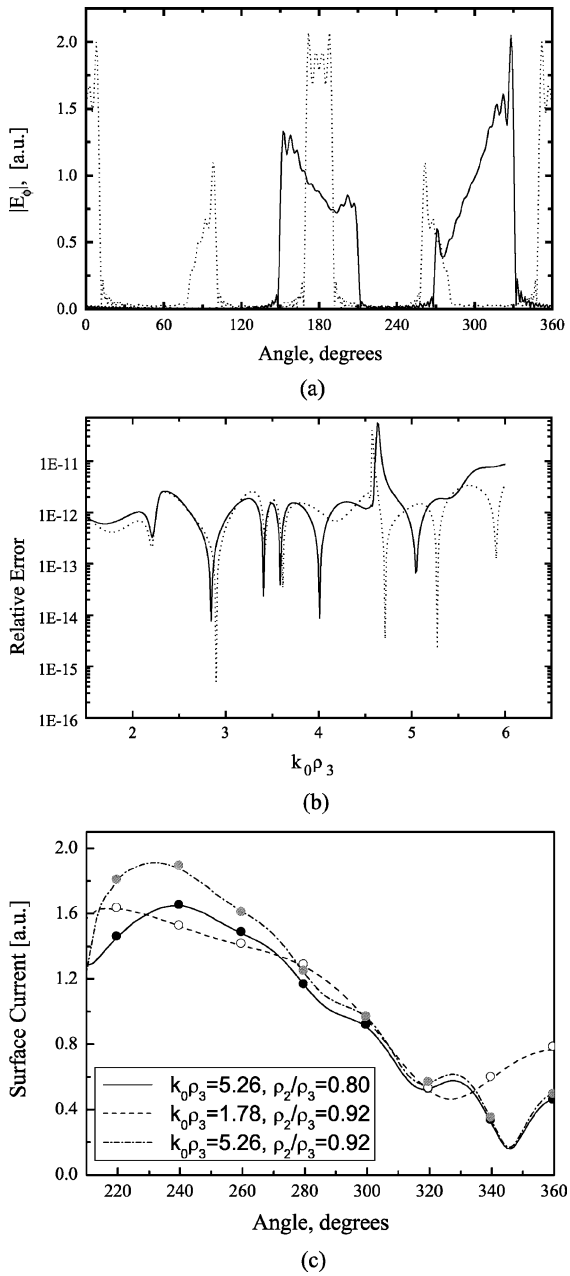

Fig. 2. On the validation of the computer code. (a) Tangential electric field at $\rho = \rho_3$ for two structures with the double-layer coating at $k_0\rho_3 = 5.26, \rho_2/\rho_3 = 0.8,\ \rho_{12}/\rho_3 = 0.75, \rho_{11}/\rho_3 = 0.7,\ \beta_1 = \pi, \beta_2 = 5\pi/3, \phi_1 = \phi_2 = \pi/3$ (solid line), $\beta_r = \pi r/2, \phi_r = \pi/9, r = 0, 1, 2, 3$ (dotted line). (b) Error of the reciprocity theorem for the structure with the same parameters as for the solid line in (a) $(\beta_{r\,(1)} = \beta_r), \phi^{\rm inc}_{(1)} = \phi^o_{(1)} = 0,\ \phi^{\rm inc}_{(2)} = \phi^o_{(2)} = \pi, \beta_{r\,(2)} = \beta_{r\,(1)} - \pi,\ \rho^o_{(1)}/\rho_3 = \rho^o_{(2)}/\rho_3 = 0.71$ (solid line) and 0.31 (dotted line). (c) Surface current on the outer surface of noncoated cylinder with $N = 1, \beta_0 = \pi$, and $\phi_0 = \pi/3$ obtained using our method (lines) and MFIE from [23, pp. 45–49] (circles).

$3.45 - 0.25i, \mu_{11} = 1)$ [22], and double-layer lossless coating whose layers are both of the same thickness and show $\varepsilon_{11} = 1.5, \mu_{11} = 1, \varepsilon_{12} = 2.5$, and $\mu_{12} = 1.5$ [7]. For convenience, we further refer to these coatings as the magnetic, electric, and double-layer coatings, respectively. The slots are assumed to be filled by the same material as the layer with $s = M$ ($\varepsilon_{2r} = \varepsilon_{1M}, \mu_{2r} = \mu_{1M}$ for all r). The most inner domain ($\rho \le \rho_{11}$) is assumed to be vacuum ($\varepsilon_{10} = \varepsilon_0, \mu_{10} = \mu_0$). Note that the effect of the coatings of the two first types on the far-zone characteristics of the field scattered by a PEC cavity with a single aperture has been studied in [5] and [6] for both TE and TM polarizations, in a wide frequency range. In [7], effect of the coating of the third type on the TM-wave penetrating through multiple apertures has been computed for several fixed frequencies. In these studies, zero thickness of the shell was assumed.

To validate the developed computer code, we checked the boundary condition for E_ϕ at $\rho = \rho_2, \rho_3$, and errors of the reciprocity theorem applied to the penetrated field. A good satisfaction of the boundary condition is observed in a wide frequency range. As an example, Fig. 2(a) shows $|E_\phi|$ at $\rho = \rho_3$ for two sample structures. Fig. 2(b) presents typical frequency dependence of the relative error in the reciprocity theorem calculated as

$$\delta_{\rm RT} = \left|1 - h_z\left(\rho^o_{(1)}, \phi^o_{(1)}, \phi^{\rm inc}_{(1)}\right) \Big/ h_z\left(\rho^o_{(2)}, \phi^o_{(2)}, \phi^{\rm inc}_{(2)}\right)\right| \tag{32}$$

where $h_z = |H^p_z|/|H^{\rm inc}_z|$ is the ratio of the penetrated and incident fields, $\rho^o_{(1)} = \rho^o_{(2)}$ and $\phi^o_{(1),(2)}$ are the coordinates of two observation points, and $\phi^{\rm inc}_{(1),(2)}$ are the incidence angles corresponding to these points, $\phi^{\rm inc}_{(1)} - \phi^o_{(1)} = \phi^{\rm inc}_{(2)} - \phi^o_{(2)}, \phi^{\rm inc}_{(2)} = \phi^{\rm inc}_{(1)} - \pi$, and $\beta_{r\,(2)} = \beta_{r\,(1)} - \pi$. Here the lower index in the brackets means the number of observation point. Good agreement has also been obtained in the far-zone field characteristics between the case of zero-thickness shell studied in [6] and the case with $\rho_2/\rho_3 = 0.9975$ studied with the aid of our model, as well as in surface current [see Fig. 2(c)].

In numerical simulations based on (4) and (5), finite number of the basis functions is used, and the infinite matrix equation given by (6) and (7) is truncated. The larger the $k\rho_1, \phi_r, {\rm Re}\varepsilon_{11}$, and ${\rm Re}\mu_{11}$, the larger the number of significant field harmonics on the rth slot, and the larger the needed number of the basis functions. Increase of ${\rm Im}\varepsilon_{11}$ and ${\rm Im}\mu_{11}$ can result in decrease of the needed value of $\max j$. In wide ranges of variation of the geometric and material parameters and frequency, including those considered in this article, it is sufficient to take $\max j = k_0\rho_3$ to obtain three stable digits in the field values [Fig. 3(a)]. This rule is kept true, at least if $\max \phi_r \le \pi/3$. The series in m and n in (1)–(3), (6), (7), (9), and (10) must be truncated at reasonable index values. For the slots, it is recommended to use $\max n \ge \max j + 2$. Throughout the paper, sufficiently large value of $\max m = 64$ was used.

The results obtained show that among the three considered coatings, the magnetic coating usually provides the best suppression of the field resonances within the whole inner domain, in a wide frequency range. Fig. 3 demonstrates the effect exerted by the magnetic coating on the field penetrated into three cylinders differing in thicknesses, numbers, and widths of the slots. The considered frequency range involves wavelengths approximately corresponding to $1.05\rho_3 \le \lambda \le 4.2\rho_3$. The curves correspond to two typical values of ρ/ρ_3. The thinner the cylinder, the thicker the inner coating needed to reduce the

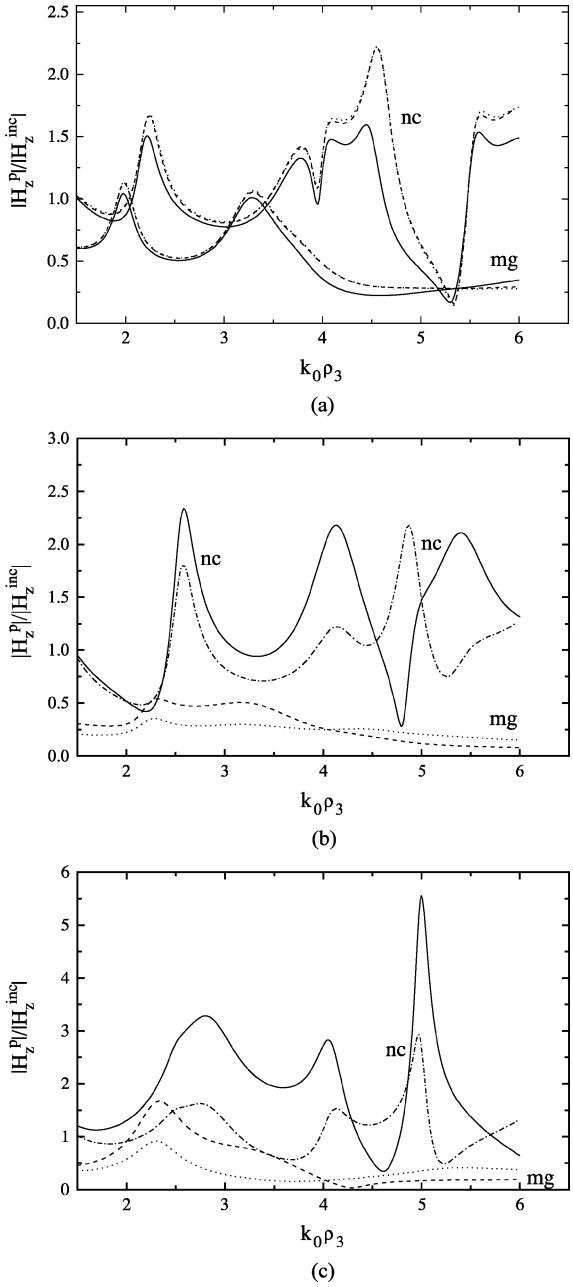

Fig. 3. Effect of magnetic coating on the field penetrated into a slotted cylinder with finite thickness with (a) $\rho_2/\rho_3 = 0.9975, \rho_{11}/\rho_3 = 0.8975, \beta_r = \pi r/2,\ \phi_r = \pi/9, r = 0, 1, 2, 3$, (b) $\rho_2/\rho_3 = 0.8, \rho_{11}/\rho_3 = 0.7, \beta_r = \pi r/2, \phi_r = \pi/9, r = 0, 1, 2, 3$, and (c) $\rho_2/\rho_3 = 0.8, \rho_{11}/\rho_3 = 0.7, \beta_1 = \pi,\ \beta_2 = 5\pi/3, \phi_1 = \phi_2 = \pi/3$. Case a: $\rho/\rho_3 = \rho_{11}/\rho_3 - 0.01$; solid, dashed, and dotted lines correspond to max $j = 1, 2$, and 3, respectively; max $n = 2 \max j$; upper curves—noncoated cylinder (nc), lower curves—magnetic coating (mg). Cases b and c: noncoated cylinder (nc) at $\rho/\rho_3 = \rho_{11}/\rho_3 - 0.01$ (solid line) and 0.31 (dashed–dotted line) and cylinder with the magnetic coating (mg) at $\rho/\rho_3 = \rho_{11}/\rho_3 - 0.01$ (dashed line) and 0.31 (dotted line). In all cases, $\phi = 0$.

penetrated field to the same level. Both decreasing the thickness of the shell and increasing the width of the slots may lead to the situation when the field amplitude inside a cylinder with a magnetic coating is even larger than that of the incident wave, within narrow frequency ranges. Despite this observation, compensation of the field enhancement is rather efficient for most

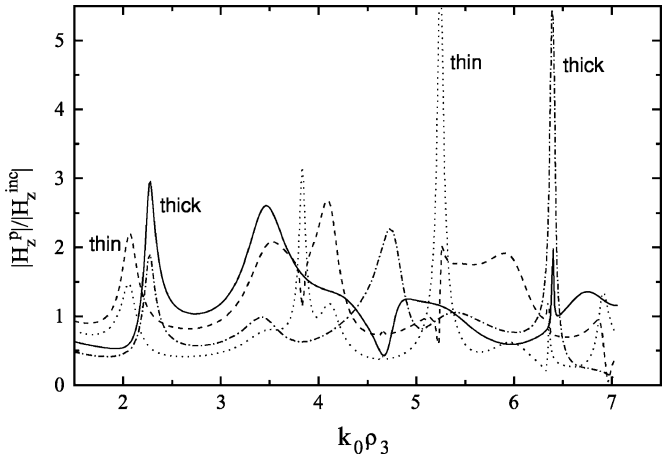

Fig. 4. Frequency dependence of the penetrated field for the thick and thin slotted cylinders with the double-layer coatings at $\rho_2/\rho_3 = 0.8, \rho_{12}/\rho_3 = 0.75, \rho_{11}/\rho_3 = 0.7$ (thick cylinder) and $\rho_2/\rho_3 = 0.9975, \rho_{12}/\rho_3 = 0.9475, \rho_{11}/\rho_3 = 0.8975$ (thin cylinder), $\beta_r = \pi r/2, \phi_r = \pi/9, r = 0, 1, 2, 3$; thick cylinder: $\rho/\rho_3 = 0.69$ (solid line) and 0.31 (dashed–dotted line); thin cylinder: $\rho/\rho_3 = 0.8875$ (dashed line) and 0.31 (dotted line), $\phi = 0$.

of the considered frequencies. Variations of number, width, and location of the slots, and coordinates of the observation point in wide ranges, do not lead to appearance of any new feature compared with those observed in Fig. 3. In the case of electric coating, resonance peaks can still be rather sharp, so that field values may be even larger than without coating. This effect is especially strong for the observation points close to $\rho = \rho_{11}$.

For a double-layer coating, the frequency dependence of the penetrated field shows some features common to those for the electric coating. However, the peaks in the former case may be even sharper than in the latter. In Fig. 4, one can see the frequency dependence of the field penetrated into the thick and thin cylinders with the double-layer coating, which was calculated for the same geometric parameters of the shell and coating thickness as in Fig. 3(a) and (b). Several sharp peaks are seen for both cylinders. Peak shift with thickness confirms their connection to the cavity resonances. The same situation occurs for the electric coating and for the noncoated cylinder. Note that the peaks of the resonances observed at $k_0\rho_3 = 5.246$ for the thin cylinder and at $k_0\rho_2 = 5.112$ for the thick cylinder are beyond the plot. For comparison, normalized cut-off wavenumbers of closed circular cylinder are $k_0\rho_3 = 5.331$ for mode TE_{12} and $k_0\rho_3 = 5.318$ for mode TE_{41}. From analysis of the field patterns, it follows that mode TE_{12} is the most influential for the mentioned peaks.

Fig. 5 compares the effects of the coatings of three types on the penetration into the thick cylinder. For the electric and double-layer coatings, the field may vary strongly at a slight frequency variation. They can be used for a narrow-band weakening/enhancement of the field inside the cylinder. For a wide-band resonance damping, the magnetic coating should be employed. This conclusion remains true in wide range of variation of geometric and material parameters.

Fig. 6 presents a comparison of the performances of thick cylinders with two wide slots and magnetic and double-layer coatings. Also shown here are the curves obtained by using the

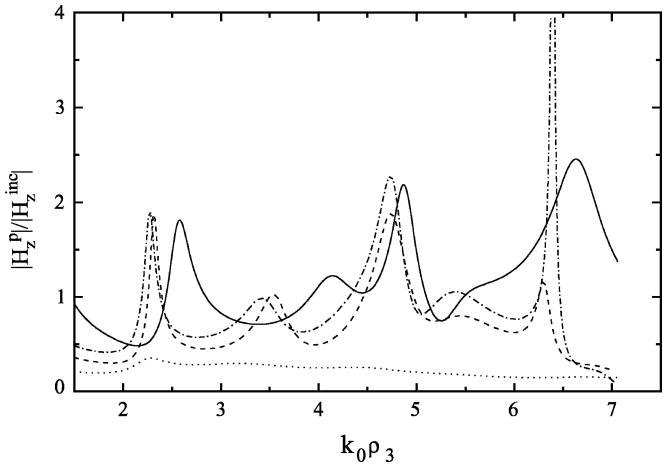

Fig. 5. Comparison of the effect of magnetic, electric, and double-layer coatings on the field penetrated into a slotted thick cylinder at $\rho_2/\rho_3 = 0.8, \beta_r = \pi r/2, \phi_r = \pi/9, r = 0, 1, 2, 3; \rho_{11}/\rho_3 = 0.7$ for the magnetic (dotted line) and electric (dashed line) coatings and for the double-layer coating (dashed–dotted line) with $\rho_{12}/\rho_3 = \rho_{11}/\rho_3 + 0.05 = 0.75$; solid line corresponds to noncoated cylinder; observation point is located at $\rho/\rho_3 = 0.31$ and $\phi = 0$.

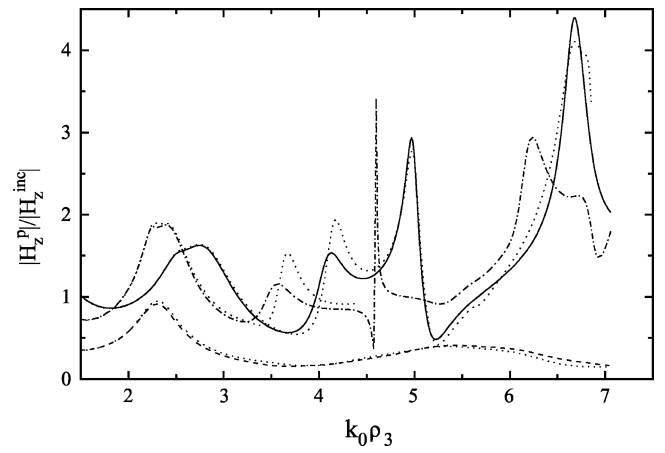

Fig. 6. Effect of magnetic (dasheded line) and double-layer (dashed-dotted line) coatings on the field penetrated into a slotted thick cylinder with two wide slots: $\beta_1 = \pi, \beta_2 = 5\pi/3, \phi_1 = \phi_2 = \pi/3$, radial dimensions and coordinates of the observation point are the same as in Fig. 5, the data for a noncoated cylinder are shown by the solid line; dotted lines correspond to the NSTW approximation.

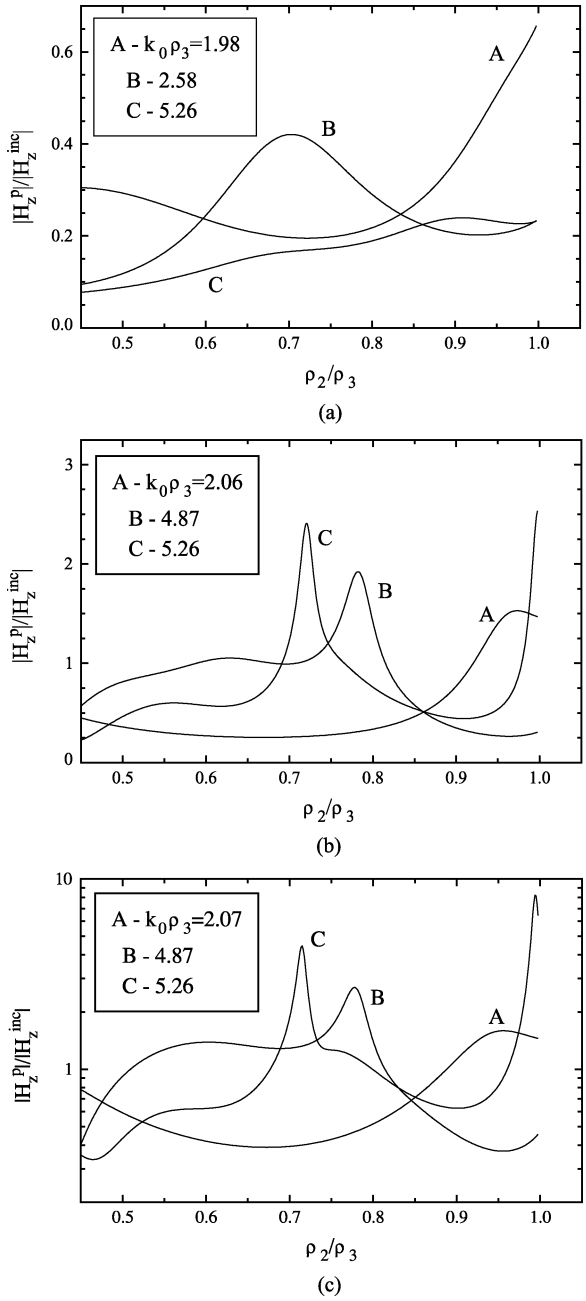

Fig. 7. Effect of cylinder thickness on the penetrated field for several values of $k_0\rho_3$ for: (a) magnetic, (b) electric, and (c) double-layer coatings. Angular geometric parameters of the shell and the coating thickness are the same as in Figs. 3(a), 3(b), 4, and 5; coordinates of the observation point are $\rho/\rho_3 = 0.31$ and $\phi = 0$; in case (c) $\rho_{12}/\rho_3 = \rho_{11}/\rho_3 + 0.05$.

NSTW approximation. Good agreement between rigorous and approximate results is observed at least at lower frequencies. The difference can be especially strong in vicinity of sharp extrema. Usually, the best agreement occurs in the case of magnetic coating, when any sharp maximum does not appear.

The effect of the thickness on the penetrated field is especially strong in the vicinity of the peaks of the frequency dependence. The field value at a fixed observation point can be strongly sensitive to a thickness variation, even if the thickness is very small (say, $\rho_2/\rho_3 > 0.97$). However, a maximum of the thickness dependence of the field usually corresponds to a maximum of its frequency dependence. As an example, Fig. 7 presents the penetrated field versus shell thickness for all three coatings. For each coating, such a dependence is presented for three typical values of $k_0\rho_3$. The value of $k_0\rho_3 = 1.98$ in Fig. 7(a) corresponds to the maximum of the frequency dependence shown in Fig. 3(a) in the case of magnetic coating. The values of $k_0\rho_3 = 2.06$ and 5.26 in Fig. 7(b), and $k_0\rho_3 = 2.07$ and 5.26 in Fig. 7(c) correspond to the vicinity of the maxima of the frequency dependence in the case of a thin cylinder with electric and double-layer coatings from Fig. 5, respectively, whereas geometric parameters of the shell are the same as in Fig. 3(a). The values of $k_0\rho_3 = 2.58$ and 4.87 correspond to the maxima on the frequency dependence in Fig. 3(b) in the case of the noncoated cylinder. Note the similarity between the dependences shown in Fig. 7(b) and (c). The main features of the thickness effect presented here for $\rho/\rho_3 = 0.31$ and $\phi = 0$ occur for other observation points as well.

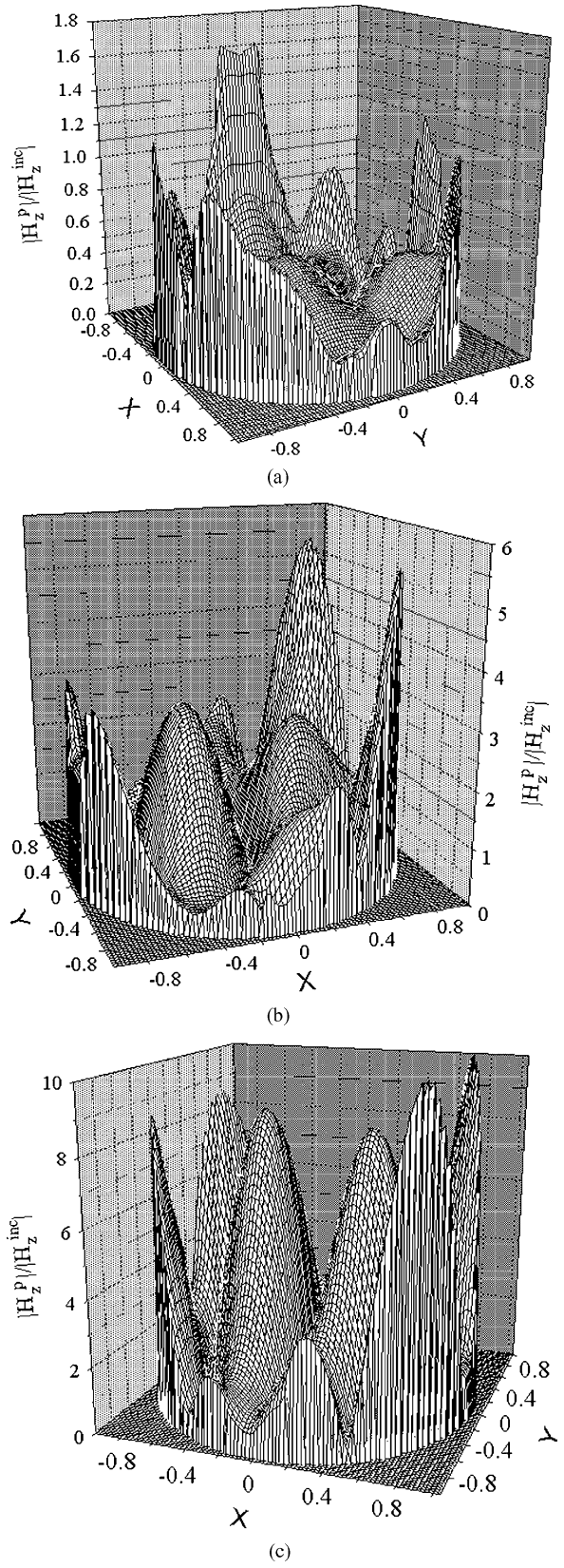

Fig. 8. Patterns of the penetrated field inside the thin cylinder at $k_0\rho_3 = 5.246$ and $\rho < \rho_2$, for: (a) magnetic, (b) electric, and (c) double-layer coatings; geometric parameters of the shell are the same as in Fig. 3(a); coating configuration is the same as in Figs. 3–7. Note that the incident wave propagates along the x-axis towards positive x. Slot apertures are centered at $x = 0, |y| = 1$ and $y = 0, |x| = 1$.

The effect of the coating thickness has also been studied for different values of the cylinder thickness. In the case of magnetic coating, the field values show a trend to decrease with increasing the coating thickness. However, the coating-thickness dependences of the field are nonmonotonic. Although in the case of double-layer coating, the effect of coating thickness on the penetrated field can be rather weak, sharp peaks may still appear corresponding to the peaks of the frequency dependence of the field. In the case of electric coating, the thickness dependence of the field has similar features with those for two other coatings.

It follows from the obtained results that if, for one of the coatings, the frequency dependence of the penetrated field has a sharp maximum at a given observation point, substantial difference between the field values for different coatings may occur at this and other observation points, provided that the frequency value is fixed. Owing to the peaks, the field pattern can strongly vary with rather slight frequency variation. Fig. 8 shows the effect of coating on the field pattern inside the thin cylinder at $\rho < \rho_2$, whereas $k_0\rho_3 = 5.246$, which corresponds to a maximum in both cases of the double-layer (Fig. 4) and electric coatings. It is seen that although the field is stronger in the coating, its values in the inner domain ($\rho \leq \rho_{11}$) can be several times of magnitude larger in comparison to the incident wave. No field enhancement is observed at $\rho \leq \rho_{11}$ in the case of magnetic coating.

IV. Conclusion

In this paper, penetration of the TE-polarized plane wave through cylindrical cavity-backed apertures has been studied by taking into account cylinder thickness. The Galerkin method has been employed to obtain a set of linear algebraic equations, which is equivalent to the inhomogeneous Helmholtz equation with the corresponding boundary conditions. The weighted Gegenbauer polynomials, which are used in Galerkin discretization, are particularly appropriate to take into account the edge condition in explicit form and obtain analytical expressions for the matrix elements. The obtained numerical results show that due to the cavity resonances, amplitude of the penetrated field can be larger than that of the incident field by several times of magnitude. The effects of inner coatings of three types have been compared. Efficient attenuation of resonances can be realized in a wide frequency range by using magnetic coating. In the case of double-layer coating, a strong enhancement of the incident field can be reached. This case is characterized by coexistence of both narrow frequency ranges, within which the field values are smaller than without coating, and sharp resonance peaks. The most important advantage of the developed model is that it can be used for arbitrary thickness of cylinder. The strongest effect exerted by the cylinder thickness on the field amplitude is observed in the vicinity of maxima in its frequency dependence. This effect cannot be neglected even for rather thin cylinders. The studied penetration effects can be interesting for engineering applications in electromagnetic compatibility and interference. The obtained results can be used, in particular, in the designs of protective shells for various communication lines.

High numerical efficiency of the developed algorithm can be further improved by applying a regularization procedure similar to [18].

REFERENCES

[1] J. R. Mautz and R. F. Harrington, "EM penetration into a conducting circular cylinder through a narrow slot, TM case," *J. Electromagn. Waves Appl.*, vol. 2, no. 3/4, pp. 269–293, 1988.

[2] ——, "EM penetration into a conducting circular cylinder through a narrow slot, TE case," *J. Electromagn. Waves Appl.*, vol. 3, no. 4, pp. 307–336, 1989.

[3] A. El-Hajj, K. Y. Kabalan, and R. F. Harrington, "Wave scattering from slit coupled cylindrical cavities with interior loading: Part II—Resonant mode expansion," *IEEE Trans. Antennas Propag.*, vol. 40, no. 2, pp. 156–161, Feb. 1992.

[4] R. W. Ziolkowski and J. B. Grant, "Scattering from cavity-backed apertures: The generalized dual series solution of the concentrically located E-Pol slit cylinder problem," *IEEE Trans. Antennas Propag.*, vol. 35, no. 5, pp. 504–528, May 1987.

[5] D. Colak, A. Nosich, and A. Altintas, "Radar cross section study of cylindrical cavity-backed apertures with outer or inner material coating: The case of E-polarization," *IEEE Trans. Antennas Propag.*, vol. 41, no. 11, pp. 1551–1559, Nov. 1993.

[6] ——, "Radar cross-section study of cylindrical cavity-backed apertures with outer or inner material coating: The case of H-polarization," *IEEE Trans. Antennas Propag.*, vol. 43, no. 5, pp. 440–447, May 1995.

[7] W.-Y. Yin, L.-W. Li, T.-S. Yeo, M.-S. Leong, and P.-S. Kooi, "The near-zone field characteristics of an E-polarization plane wave penetrating through cylindrical multiple apertures (non) coated with lossy and lossless media," *IEEE Trans. Electromagn. Compat.*, vol. 44, no. 2, pp. 329–337, May 2002.

[8] A. I. Nosich, "Green's function dual series approach in wave scattering by combined resonant scatterers," in *Analytical and Numerical Methods in EM Wave Theory*, M. Hashimoto, M. Imeden, and O. A. Tretyakov, Eds. Tokyo, Japan: Sci. House, 1993, pp. 419–469.

[9] T. M. Wang, A. Cuevas, and H. Ling, "RCS of a partially open rectangular box in the resonator region," *IEEE Trans. Antennas Propag.*, vol. 38, no. 9, pp. 1498–1504, Sep. 1990.

[10] J. D. Shumpert and C. M. Butler, "Penetration through slots in conducting cylinders—Part 1: TE case," *IEEE Trans. Antennas Propag.*, vol. 46, no. 11, pp. 1612–1621, Nov. 1998.

[11] ——, "Penetration through slots in conducting cylinders—Part 2: TM case," *IEEE Trans. Antennas Propag.*, vol. 46, no. 11, pp. 1622–1628, Nov. 1998.

[12] Y. C. Noh and S. D. Choi, "TM scattering from hollow slotted circular cylinder with thickness," *IEEE Trans. Antennas Propag.*, vol. 45, no. 5, pp. 909–910, May 1997.

[13] G. Manara, A. Monorchio, and G. Pelosi, "Electromagnetic scattering from longitudinally corrugated cylinders," *IEEE Trans. Antennas Propag.*, vol. 45, no. 11, pp. 1700–1701, Nov. 1997.

[14] M. G. Andreasen, "Scattering from parallel metallic cylinders with arbitrary cross sections," *IEEE Trans. Antennas Propag.*, vol. 12, pp. 746–754, Nov. 1964.

[15] F. Xiao and H. Yabe, "An efficient finite element—Integral equation method for electromagnetic scattering from metallic cylinders with arbitrary cross sections," *IEICE Trans. Electron.*, vol. E81-C, no. 10, pp. 1648–1654, Oct. 1998.

[16] W.-Y. Yin, L.-W. Li, T.-S. Yeo, and M.-S. Leong, "Multiple penetration of a TEz-polarized plane wave into multi-layered cylindrical cavity-backed apertures," *IEEE Trans. Electromagn. Compat.*, vol. 42, no. 4, pp. 330–338, Nov. 2000.

[17] A. Erdelyi, *Higher Transcendental Functions*. ch. 2, vol. 2, New York: McGraw-Hill, 1953.

[18] V. P. Lyapin, M. B. Manuilov, and G. P. Sinyavsky, "Quasi-analytical method for analysis of multisection waveguide structures with step discontinuities," *Radio Sci.*, vol. 31, no. 6, pp. 1761–1772, Nov.–Dec. 1996.

[19] K. Schuenemann, A. E. Serebryannikov, and O. E. Vasylchenko, "Analysis of non-periodic azimuthally corrugated structures by coupled-integral-equations technique," *Int. J. Electron. Commun. (AEÜ)*, vol. 58, no. 2, pp. 79–85, Feb. 2004.

[20] M. Abramowiz and I. A. Stegun, Eds. *Handbook of Mathematical Functions,* Ser. National Bureau of Standards, *Appl. Math. Series*, 1972.

[21] C. S. Lee and S. W. Lee, "RCS of a coated circular waveguide terminated by a perfect conductor," *IEEE Trans. Antennas Propag.*, vol. 35, no. 4, pp. 391–398, Apr. 1987.

[22] R. F. Harrington, *Time–Harmonic Electromagnetic Fields*. New York: McGraw-Hill, 1961.

[23] A. F. Peterson, S. L. Ray, and R. Mittra, *Computational Methods for Electromagnetics*. Oxford, U.K.: Oxford Univ. Press, 1997.

Andriy E. Serebryannikov (M'00) was born in Kharkov, Ukraine, in 1967. He received the Enginner-Physisist degree from Kharkov Polytechnic University, Kharkov, Ukraine, in 1990 and the Ph.D. degree in radio physics from the Kharkov National University, Kharkov, Ukraine, in 1996.

Since 1992, he has been with Institute of Radio Astronomy of National Academy of Science of Ukraine, Kharkov. From 1999 to 2002 and since 2004, he has been with the Technische Universitaet Hamburg–Harburg, Hamburg, Germany. He has published more than 50 journal and conference papers. His current research interests include the electromagnetic theory of slot structures, theory and applications of photonic crystals and of metamaterials, inhomogeneous media, and microwave vacuum tubes.

Alexander I. Nosich (M'94–SM'95–F'04) was born in Kharkov, Ukraine, in 1953. He received the M.S., Ph.D., and D.Sc. degrees in radio physics from the Kharkov National University, Kharkov, Ukraine, in 1975, 1979, and 1990, respectively.

Since 1979, he has been with Institute of Radio-Physics and Electronics of National Academy of Sciences of Ukraine, Kharkov, Ukraine and is currently a Leading Scientist. His research interests include the method of analytical regularization, propagation, and scattering of waves in open waveguides, simulation of semiconductor lasers and antennas, and the history of microwaves. Since 1992, he has held numerous guest fellowships and professorships in the EU, Japan, Singapore, and Turkey.

In 1990, he was one of the initiators and a Technical Committee Chairman of the International Conference Series on Mathematical Methods in Electromagnetic Theory. In 1995, he organized an IEEE AP-S Chapter in East Ukraine, the first one in the former USSR. From 2001 to 2003, he represented the Ukraine, Poland, and the Baltic States in the European Microwave Association.